aerospace

MDPI

Article

A Parallelized Genetic Algorithm to Evaluate Asteroid Impact Missions Using Electric Propulsion

Kamesh Sankaran [1,*], Scott A. Griffith [2], Noah C. Thompson [1], Matthew D. Lochridge [1] and Andrew S. O'Kins [2]

[1] Department of Engineering & Physics, Whitworth University, Spokane, WA 99251, USA; nthompson22@my.whitworth.edu (N.C.T.); mlochridge22@my.whitworth.edu (M.D.L.)
[2] Department of Mathematics & Computer Science, Whitworth University, Spokane, WA 99251, USA; sgriffith@whitworth.edu (S.A.G.); aokins22@my.whitworth.edu (A.S.O.)
* Correspondence: ksankaran@whitworth.edu

Abstract: A streamlined genetic algorithm was developed and implemented on a GPU to evaluate low-thrust trajectories of spacecraft propelled by an ion thruster. It was then applied to examine the utility of a specific thruster for an asteroid impact mission. This method was validated by comparing impact speeds of non-thruster results with the DART mission, which does not significantly use the equipped ion thruster. Then, by utilizing the ion thruster for prolonged periods, this model demonstrated the possibility of significant increases in the impact speed and significant decreases in the trip times. This specific test case was used to examine the utility of the model and, by methodically varying relevant variables, this article shows the influence of the genetic algorithm on the results. By examining a range of electrical power levels, the results presented here provide hints as to the possible effects of spacecraft design trade-offs on impact speed. The analysis of the effects of the algorithm on the results and the evaluation of thruster operating parameters indicate the applicability of this model to a variety of spaceflight missions.

Keywords: electric propulsion; asteroid mission; genetic algorithm

Citation: Sankaran, K.; Griffith, S.A.; Thompson, N.C.; Lochridge, M.D.; O'Kins, A.S. A Parallelized Genetic Algorithm to Evaluate Asteroid Impact Missions Using Electric Propulsion. *Aerospace* **2022**, *9*, 116. https://doi.org/10.3390/aerospace9030116

Academic Editors: Mikhail Ovchinnikov and Dmitry Roldugin

Received: 6 January 2022
Accepted: 21 February 2022
Published: 24 February 2022

1. Introduction

Missions to asteroids using electric propulsion have been studied for various destinations and thruster options [1–7]. Asteroid impact missions, such as the Double Asteroid Redirection Test (DART) [8], employ a kinetic impactor to change the orbit of an asteroid. Various publications [9–12] have evaluated the use of the NASA Evolutionary Xenon Thruster (NEXT) [13] to evaluate design options for the DART mission. The DART mission was launched on 24 November 2021 to impact the Didymos asteroid system 430 days later with an impact speed of 6.58 km/s. Ozimek and Atchison developed a low-thrust trajectory concept using the NEXT thruster if the DART mission was to be launched as a ride-share from a geostationary transfer orbit (GTO) [11]. In the same vein, Sarli et al. [12] evaluated its cruise phase using the NEXT-Commercial (NEXT-C) thruster. Though the DART mission has abandoned the commercial ride-share approach in favor of a designated launch vehicle that has put the spacecraft directly on an earth-escape trajectory, Refs. [11,12] provide a starting point for our work to demonstrate an alternative method for analyzing such missions.

The objective of this article is to demonstrate the utility of a parallelized baseline genetic algorithm by evaluating the effect of a specific thruster on an asteroid impact mission. We validated our algorithm by comparing its results to the DART mission, whose relevant details are provided in Sections 4.1 and 4.2. Genetic algorithms have been used extensively to optimize spacecraft trajectories for various missions [14–17]. Among methods that calculate differential equations of motion consistently, genetic algorithms offer an advantage of using diversity in the parameter space to dynamically tune solutions to optimize the trajectory and avoid local minima. However, genetic algorithms are inefficient

in serial computation because such methods can only compute one individual simulation at a time. We have demonstrated that parallelizng a baseline genetic algorithm can be effective for evaluating trajectory options for such missions, even on an entry-level desktop GPU system. As discussed in Section 4.1, we focused on the heliocentric portion of the DART mission because the launch vehicle for the evaluated mission has $C_3 > 0$. Following Ref. [11], we set the net launch mass of the spacecraft to be 650 kg, with a dry mass $\geq$500 kg and propellant mass $\leq$150 kg.

2. NEXT-C Ion Thruster

Low-thrust propulsion systems pose challenges for analytical trajectory optimization methods because their long-term operation with intermittent coasting can affect the motion of the spacecraft in more ways than impulsive high-thrust maneuvers. NASA's Evolutionary Xenon Thruster—Commercial (NEXT-C) [18] is a viable candidate for many deep space missions and, therefore, it is a suitable candidate to demonstrate the capabilities of our genetic algorithm for asteroid impact missions. In this study, we treated the maximum electrical power available to the thruster from the solar panel as $P_{\text{max}} = 7330$ W. To account for the restrictions in a mission's actual power source, we examined a range of available power levels, $0 < P_{\text{source}} < P_{\text{max}}$ in Section 6.2.2, to discuss how changes to the spacecraft design could affect the thruster's utility. The input power from the solar panels to the thruster was set to decrease with distance from the Sun as $P_{\text{in}}(t) = P_{\text{source}}/(\mathscr{r}(t)/1\text{ AU})^2$, where $\mathscr{r}(t) = \sqrt{r(t)^2 + z(t)^2}$ is the magnitude of separation. The data from Fisher et al. [19] was used to set the propellant flow rate as $\dot{m}(P_{\text{in}}(t))$ and the thrust efficiency as $\eta(P_{\text{in}}(t))$. When $\dot{m}(t) > 0$, the thrust power was $P_{\text{th}}(t) = \eta(t)P_{\text{in}}(t)$ and the available thrust was $F_{\text{th}}(t) = \sqrt{2P_{\text{th}}(t)/\dot{m}(t)}$.

3. Mission Parameters

The focus of our work was on the portion of the trip from the Earth's sphere of influence (ESOI) to impact. We defined a distinct option for the trip to be comprised of the following variables: the triptime (T), the angular location of the spacecraft in the ecliptic plane at departure from ESOI (α), and the in-plane and off-plane angles of the velocity at departure from ESOI (β, ζ), along with the Fourier coefficients for thrusting ($\gamma(t), \tau(t)$) and the input to the coasting function ($\psi(t)$). Therefore, each potential trajectory was uniquely identified by this set of parameters:

$$\left[T; \alpha; \beta; \zeta; \underbrace{a_{0,\gamma}, a_i, b_i \ldots}_{\gamma(t)}; \underbrace{a_{0,\tau}, a_1, b_1 \ldots}_{\tau(t)}; \underbrace{a_{0,\psi}, a_k, b_k \ldots}_{\psi(t)}\right]. \tag{1}$$

Though there are many ways to estimate the coasting segments and the thrusting angles, we chose a Fourier series approximation for them because the coefficients can be optimized using a genetic algorithm. In contrast to other studies [20] that have estimated the resulting trajectory of the spacecraft ($r(t)$ and $\theta(t)$) using Fourier series, we used Fourier series here to estimate the input parameters [21] and obtained the trajectory as a result of Newtonian mechanics, as discussed in Section 4. The thrusting angles in the plane ($\gamma(t)$) and off-the plane ($\tau(t)$), as well as the input to the coasting function ($\psi(t)$), were calculated in the following way:

$$\gamma(t) = a_{0,\gamma} + \sum_{i=1}^{3} a_i \cos\left(2\pi i \frac{t}{T}\right) + b_i \sin\left(2\pi i \frac{t}{T}\right), \tag{2}$$

$$\tau(t) = a_{0,\tau} + a_1 \cos\left(2\pi \frac{t}{T}\right) + b_1 \sin\left(2\pi \frac{t}{T}\right), \tag{3}$$

$$\psi(t) = a_{0,\psi} + \sum_{k=1}^{2} a_k \cos\left(2\pi k \frac{t}{T}\right) + b_k \sin\left(2\pi k \frac{t}{T}\right). \tag{4}$$

These individual Fourier coefficients used to calculate $\gamma(t)$, $\tau(t)$, and $\psi(t)$ are a part of the "chromosome" in Equation (1). To optimize propellant use, the thruster was turned on/off in the following fashion. The optimization process described in Section 5 was used to obtain the coefficients of the Fourier series to generate an input function, $\psi(t)$, that generated a normalized coasting function, $f_{\text{coast}}(\psi(t)) = \sin^2(\psi(t))$, such that $0 \leq f_{\text{coast}} \leq 1$. The thruster was turned on if $f_{\text{coast}}(\psi(t)) > 0.5$; otherwise, the spacecraft traveled only under the gravitational influence of the Sun.

4. Parallelized Evaluation Process

Each option for the mission, with its unique set of parameters, was evaluated as to whether it would impact the asteroid in the following manner. Because this study only examined the heliocentric portion of the trip, we employed a standard Newtonian model, with gravity of the Sun and thrust as the only forces on the spacecraft. Though several additional forces on the spacecraft, such as perturbations due to the gravity of other objects in the solar system and solar radiation pressures [22], must be accounted for to achieve accurate orbital determination, we considered only the gravitational force of the Sun here. Because our objective was to evaluate the effect of an ion thruster on the mission, the Sun's gravity had the most significant influence on this calculation. The motion of the spacecraft was described using six coupled ordinary differential equations for position and velocity as a function of time. The acceleration due to thrust was $a_{\text{th}}(t) = F_{\text{th}}(t)/(m_0 - \int \dot{m}(t)dt)$, where the total mass at launch was set to $m_0 = 650$ kg.

4.1. Launch

The initial values of position (r, θ, z) and velocity (V_r, V_θ, V_z) were set in the following manner in cylindrical coordinates. Based on trip time (initially a random guess between 1.0–1.5 years, as shown in Table 1, to allow comparisons with the DART mission's trip time of 1.19 years) and the fixed impact date at the asteroid (discussed in Section 4.2), the motion of the Earth around the Sun was calculated in reverse to determine the spacecraft's location at launch. Then, at the radius of the sphere of influence of the Earth–Moon system compared to the Sun, r_{ESOI}, the angular position of the spacecraft, α, on the ecliptic plane ($z = 0$) can be optimized by the genetic algorithm. Thus, the position of the spacecraft at $t = 0$ was specified to be

$$r_{\text{ini/Sun}} = r_{\text{Earth/Sun}} + r_{\text{ESOI}} \cos(\alpha), \tag{5}$$

$$\theta_{\text{ini/Sun}} = \theta_{\text{Earth/Sun}} + \arcsin\left(\sin(\pi - \alpha)\frac{r_{\text{ESOI}}}{r_{\text{Earth/Sun}}}\right), \tag{6}$$

$$z_{\text{ini/Sun}} = z_{\text{Earth/Sun}}. \tag{7}$$

The specific energy provided to the spacecraft by the Falcon 9 launch vehicle was assumed to be $C_3 = 4.676$ km^2 s^{-2} (personal communication with Justin Atchison). We discuss the effect of varying this launch energy in Section 6.2.4. The given C_3 energy determined the speed of the spacecraft as it left the Earth's sphere of influence, $V_{\text{ESOI}} = \sqrt{C_3}$. The optimization algorithm provided values for the in-plane angle of velocity, β, and the off-plane angle of velocity, ζ, for each mission option. Thus, the initial velocity of the spacecraft was specified to be

$$V_{r,\text{ini/Sun}} = V_{r,\text{Earth/Sun}} + V_{\text{ESOI}} \sin\beta \cos\zeta, \tag{8}$$

$$V_{\theta,\text{ini/Sun}} = V_{\theta,\text{Earth/Sun}} + V_{\text{ESOI}} \cos\beta \cos\zeta, \tag{9}$$

$$V_{z,\text{ini/Sun}} = V_{z,\text{Earth/Sun}} + V_{\text{ESOI}} \sin\zeta. \tag{10}$$

Table 1. Range of mission parameters.

Variable	Range
T	1.0–1.5 yrs
α	$\pm\pi$ rad
β	0–π rad
ζ	$\pm\pi/2$ rad
γ	$\pm\pi$ rad
τ	$\pm\pi/2$ rad
ψ	$\pm\pi$ rad

4.2. Impact

We set the final value of time in our calculations to be 30 September 2022 19:54:55 UTC, which is the time of impact of the DART baseline mission design, to allow for comparison of the results. While the DART mission aims to impact the moonlet of the system, our calculations ended at the center of mass of Didymos as this information is readily available (https://ssd.jpl.nasa.gov/sbdb.cgi, accessed on 6 January 2022). Because our goal is to demonstrate the utility of an algorithm by using the DART mission as an example and not to make specific recommendations for the mission, this was a reasonable target for our purposes. At the end of its triptime (T), the distance of the spacecraft to the center of mass of the asteroid, δl, was set as its cost,

$$\text{Cost} = \delta l = \sqrt{(\Delta r)^2 + (\Delta(r\theta))^2 + (\Delta z)^2}, \tag{11}$$

where the Δ in Equation (11) denotes the difference in the position of the asteroid and the spacecraft in each dimension. The desired tolerance was set to be $\epsilon = 10^{-10}$ AU $\simeq 15$ m (in comparison, in the Didymos system, the primary asteroid is 780 m in diameter and its satellite is 160 m in diameter in an orbit of diameter 1000 m around the primary). The only objective of the algorithm was to achieve $\delta l \leq \epsilon$ and this was considered "impact". We then compared the speed of the spacecraft (relative to the asteroid-centered EME2000 frame) at impact to the baseline value of the DART mission, $|\Delta\vec{V}|_{\text{imp,DART}} = 6.58$ km/s (personal communication with Justin Atchison).

4.3. Heliocentric Trip

Starting with the initial conditions for position and velocity of the spacecraft, the Newtonian equations of motion were numerically integrated using a 7-step Runge–Kutta algorithm [23]. Conservation of mechanical energy (kinetic + gravitational potential energy) and angular momentum were monitored to track errors in the numerical methods. The process was parallelized in the following manner. The position and velocity of the Earth were calculated a priori for a large range of potential trip times, T. Then, a large number of independent options for the mission, each with its unique set of parameters specified by Equation (1), were generated and passed on to the GPU as independent threads for computation. Each of those options was evaluated in parallel using the equations of motion, and each mission design was verified at the end of its independent integration to check if it met its only objective (described in Section 4.2), i.e., "Did the spacecraft arrive at the asteroid within $\delta l < 10^{-10}$ AU?". Depending on this Boolean result, these mission parameters were then manipulated by the optimization process described in Section 5 to generate a new set of parameters to be processed.

5. Genetic-Algorithm-Based Optimization of Parameters

We developed a parallelized genetic algorithm on a GPU to optimize the parameters described in Section 3, subject to the conditions described in Section 4. Each thread was considered an "individual" (a distinct mission option) with its "chromosome" that contained the set of mission parameters (Equation (1)) to be optimized. The number of

individuals in the population was set to the number of cores in the GPU (2880 for the NVIDIA Tesla K40 used in this work). Because the order of each Fourier series for γ, τ, and ψ was configurable for each run, the sizes of chromosomes were determined at run-time. The parameters of the initial pool of individuals, the first generation, were seeded randomly within the limits shown in Table 1. Because the convergence criterion is the same as the single objective function (Equation (11)), the complexity of this approach is greatly reduced compared to the more advanced genetic algorithms used in Refs. [16,17], and, thus, our method represents a "baseline" genetic algorithm for this problem. On a regular desktop with 1 CPU and a NVIDIA Tesla K40 GPU (several generations behind the state-of-the-art), a typical result shown in Section 6 took 10–15 min of run time.

5.1. Crossover

Starting with the initial conditions, and using a combination of thrusting and coasting, each mission option was evaluated in parallel using the equations of motion to calculate its cost function (Equation (11)). When all individuals completed their integration, it marked the end of a generation. The individuals in the top 50% of the lowest δl were allowed to continue to the next generation, and the rest were replaced with newly generated individuals. To do this, all the previous generation's individuals were sorted into two pools based on two criteria: 1. lowest δl and 2. highest ΔV_{imp}. A new pool of "parents" was then created from these two sorted pools based on the sorting ratio, Φ (e.g., $\Phi = 0.25$ chose 25% of parents based on lowest δl and 75% based on highest ΔV_{imp}). This new pool of "parents" was then shuffled to have a mixture of the two types of chosen individuals for crossover. To generate a new individual, two "parents" were used in three distinct crossover methods: 1. Random, 2. Average, and 3. Bundled Random. The Random crossover chose a gene at random from one of the parents to fill in the new chromosome. The Average crossover took the average of each of the parent's genes to form the new chromosome. The Bundled Random crossover worked similar to the Random method but kept each of the Fourier coefficient sets (γ, τ, and ψ) intact, each one coming from one of the two parents. For each parent pair, eight new individuals were created: two mirrored individuals from the Random method, two individuals from the Average method, and four individuals from the Bundled Random method.

5.2. Mutations

After crossover, the new individuals underwent a potential mutation process. The chance of any one gene mutating was μ, and a specified compounding mutation rate was applied for each individual. If one mutation was performed, that rate was applied again for a second gene to mutate, and so on, such that $0 < \mu < 1$. If selected for mutation, a gene's mutation was scaled by an annealing factor (described in Section 5.3). The crossover and mutation processes continued to change the composition of the population until the best individual met the objective ($\delta l < 10^{-10}$ AU). Because of the simplicity of the cost function and the singular objective, this streamlined method did not require computationally expensive pair-wise comparisons of multi-objective algorithms [16].

5.3. Annealing

An anneal factor, $0 \leq \omega \leq 1$, was used to guide the genetic mutations towards convergence. If $\omega \to 1$, the mutations were under-damped and the changes from one generation to the next were too large to make any necessary small refinements; conversely, $\omega \to 0$ caused the mutations to be over-damped. With $\omega = 0.5$, convergence was consistently reached with $\mathcal{O}(10^3)$ generations, and most of the results presented in Section 6 converged in $\mathcal{O}(10^2)$ generations.

6. Results and Discussion

We will now examine the ability of this genetic algorithm to evaluate the effect of the ion thruster on the mission. In doing so, we can also understand the influence of the variables in the genetic algorithm on the results.

6.1. Baseline

To make a reasonable comparison with the baseline of the DART mission, we first obtained results without using the propulsion provided by the NEXT-C ion thruster. We used four independent ways to verify that the thruster did not affect the solution: (1) Set $f_{\text{coast}} = 0$ and ensure that the thruster was never turned on, (2) set the total available fuel mass to zero, (3) set the available power below the lowest throttle point to ensure that the propellant flow rate was always zero, and (4) set available power to zero to ensure that thrust was always zero.

This model readily converged under these restrictions and provided multiple solutions that resembled the DART mission within 1% of the baseline values of trip time of 434.75 days and impact speed (relative to the asteroid) of 6.58 km/s. A small sample of such solutions is shown in Table 2.

Table 2. Sample earth escape parameters and impact speeds (without using the NEXT-C thruster).

α (Rad)	β (Rad)	ζ (Rad)	T (Days)	ΔV_{imp} (km/s)
−1.8	1.7	−0.9	435.69	6.64
−1.6	1.7	−0.9	435.44	6.63
−1.5	1.8	−0.9	435.33	6.62
−0.8	1.8	−0.9	434.55	6.58
−0.6	1.9	−0.9	434.16	6.57
−0.3	1.9	−0.9	433.72	6.57
0.1	1.9	−0.9	432.77	6.59
0.3	1.9	−0.9	432.41	6.60
0.5	1.9	−0.9	432.21	6.62

6.2. Comparable Trip Time

We then examined how a significant use of the ion thruster affected the mission. Because the genetic algorithm iterated through a range of trip times, the limits set on the allowable values of T determined the options evaluated and, therefore, the results obtained. We now present the results when we specified $1.0 < T < 1.5$ years to allow for comparison with the DART mission's trip time of 1.19 years. Four notable variables in the model influence the results: the available propellant mass (m_{prop}), the available power (P_{source}), the ratio Φ, and the launch energy C_3. The effects of each of these four variables are presented and discussed in this subsection. The results of those variations are shown in Figures 1–4, and they indicate that each scenario provides options to reduce the trip time and also significantly increase the impact speed at the asteroid compared to the DART baseline.

6.2.1. Varying Available Propellant Mass

While the total spacecraft mass at ESOI was fixed at $m_\circ = 650$ kg, we examined the results of varying the available propellant in the range of $0 < m_{\text{prop}} < 150$ kg (thus, $500 < m_{\text{dry}} < 650$ kg). As expected, Figure 1 shows that an increased use of the propellant by the ion thruster resulted in an increased speed of impact. With $P_{\text{max}} = 7330$ W, $C_3 = 4.676$ km^2 s^{-2}, and $\Phi = 0.5$, allowing $m_{\text{prop}} = 150$ kg enhanced the impact speed by 5 km/s more than the DART baseline of 6.58 km/s.

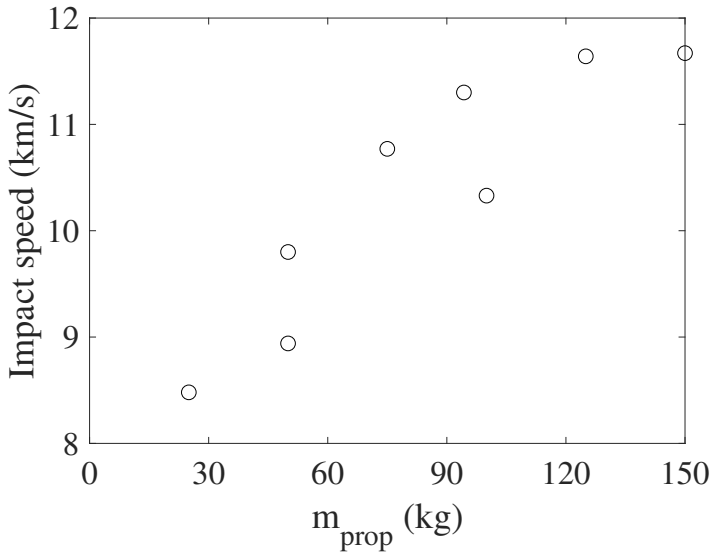

Figure 1. Variation of the impact speed with propellant mass ($C_3 = 4.676$ km^2 s^{-2}, $P_{\text{source}} = 7330$ W, and $\Phi = 0.5$).

6.2.2. Varying Available Power

We conducted a series of calculations that examined the effect of varying the available power source in the range of $0 < P_{\text{source}} < P_{\text{max}} = 7330$ W. As expected, Figure 2 shows that an increased availability of electrical power resulted in an increased speed of impact. With $C_3 = 4.676$ km^2 s^{-2}, $m_{\text{prop}} = 150$ kg, and $\Phi = 0.5$, using P_{max} enhanced the impact speed by >5 km/s compared to the DART baseline. Though actual mission constraints may not allow for power levels up to P_{max}, this result indicates the potential benefit of examining the spacecraft design trade-offs towards this end.

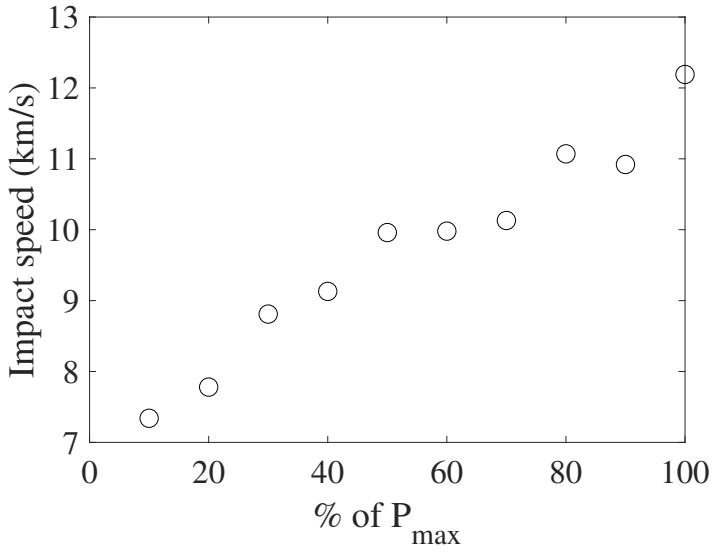

Figure 2. Variation of the impact speed with power as a % of P_{max} ($C_3 = 4.676$ km^2 s^{-2}, $m_{\text{prop}} = 150$ kg, and $\Phi = 0.5$).

6.2.3. Varying Survivor Selection

We varied Φ, the fraction of "parents" chosen based on low values of δl versus high values of ΔV_{imp}, to examine if lowering Φ would lead to more results with higher impact speeds. The results, shown in Figure 3, reveal that the decreasing $\Phi \rightarrow 0$ does not lead to a monotonic increase in the impact speed. This was because, as Φ dropped below 0.2, the

resulting genetic pool in which >80% of its population was *not* chosen based on its ability to meet the cost function was less likely to produce an offspring that converged. Therefore, as seen in Figure 3, the range of $0.1 < \Phi < 0.3$ was most likely to produce results with high-impact speeds while also converging consistently within the constraints specified in Table 1.

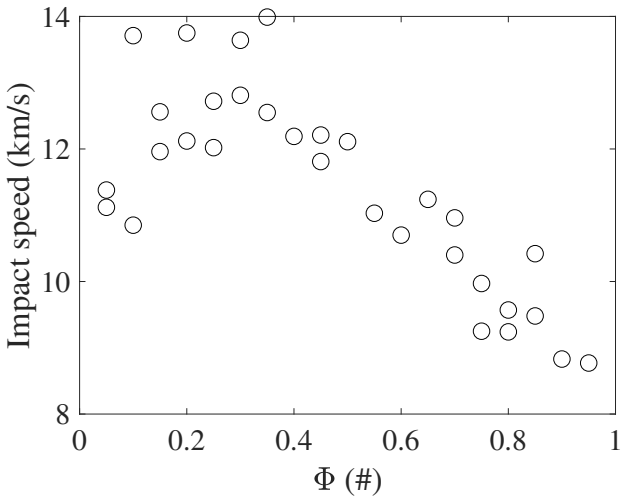

Figure 3. Variation of the impact speed with the selection variable, Φ ($C_3 = 4.676$ km^2 s^{-2}, $P_{\text{source}} = 7330$ W, and $m_{\text{prop}} = 150$ kg).

However, many of the results with highest impact speeds in Figure 3 often took a path of going inside the Earth's orbit ($r < 1$ AU) for a portion of the trip. If the genetic algorithm was allowed a low constraint of $r_{\text{min}} = 0.5$ AU, it even produced results with $\Delta V_{\text{imp}} > 18$ km/s. Though these options are undesirable due to many engineering constraints, these results indicate that the genetic algorithm functioned as intended.

6.2.4. Varying Launch Energy

We examined the effect of the launch energy by reducing it up to $C_3 = 3.04$ km^2 s^{-2} (65% of the baseline). The results shown in Figure 4 indicate the expected trend of decrease in impact speed with decreasing launch energy. It is noteworthy that, with even a 35% reduction in launch energy, the ion thruster allowed the spacecraft to impact the target with a speed > 8 km/s (when $m_{\text{prop}} = 150$ kg, $P_{\text{source}} = 7330$ W, and $\Phi = 0.2$).

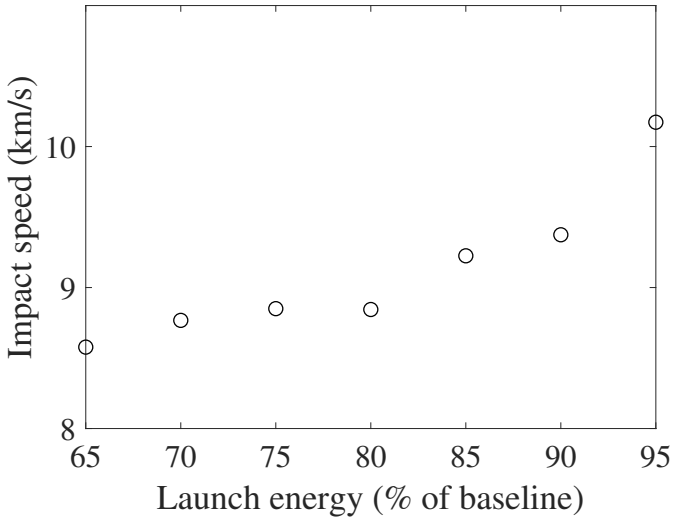

Figure 4. Variation of the impact speed with launch energy as a % of the baseline ($m_{\text{prop}} = 150$ kg, $P_{\text{source}} = 7330$ W, and $\Phi = 0.2$).

6.3. Short Trip Time

We also examined the possibility of scenarios with drastically lower trip times. Because the trip time was one of the parameters in Equation (1) that defined a distinct mission option, the optimization configuration specified its maximum and minimum bounds. When the maximum bound was reduced significantly, for example, to $0.1 < T < 0.5$ years instead of the DART mission baseline of $T = 1.19$ years, the genetic algorithm yielded very different options. The sample result in Figure 5 used 16.6 kg of propellant, took 52.98 days of trip time, and resulted in an impact speed of 7.46 km/s (with $P_{\text{source}} = 7330$ W and $\Phi = 0.5$). Such radical options may not be desirable for an actual mission but are, nevertheless, helpful to understand the workings of this model and to envision some theoretical possibilities.

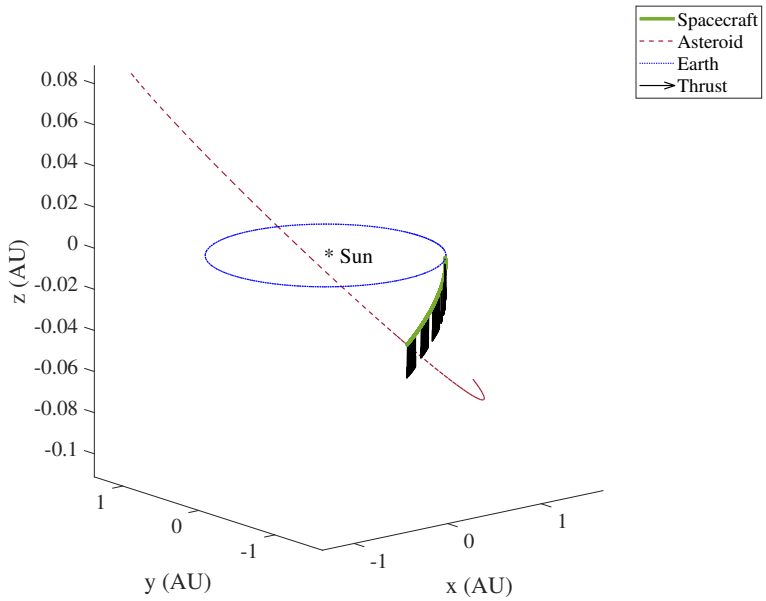

Figure 5. Orbit of the spacecraft, with the thrust vectors, from the earth to the asteroid for a very short trip. This option had a high value of ζ at launch, $T = 52.98$ days, $m_{\text{prop,used}} = 16.6$ kg, and $\Delta V_{\text{imp}} = 7.46$ km/s.

7. Concluding Remarks

We have presented a parallelized and simplified genetic algorithm to evaluate propulsion options for low-thrust spacecraft trajectories and have applied it to examine the utility of the NEXT-C thruster for an asteroid impact mission. The highest impact speed was achieved when about 20% of the survivors were chosen based on proximity to the target and 80% based on impact speed. Our results show that thrusting for prolonged periods with 50–150 kg of xenon propellant will offer significant mission alternatives and allow the spacecraft to impact the target with a significantly greater speed (>13 km/s) or make the trip in a significantly shorter time compared to the mission baseline. We also found that the ion thruster can compensate for the loss of launch energy; the impact speed was higher than the no thruster case even when the launch C_3 was cut by 35%. However, there are three significant reasons to refrain from drawing direct inferences from this article to actual missions such as the DART. First, though the real mission requires a specified 3-D velocity vector at impact, our work evaluated only a scalar impact speed relative to the asteroid. This limits any direct comparisons with or implications for the actual mission. However, Ref. [12] showed that optimizing the kinetic energy at impact (a scalar) was a useful objective that yielded many locally optimal solutions for that mission; therefore, it is reasonable to expect solutions that maximize v_{imp} to also be relevant for maximizing v_{imp}^2. Second, our calculations examined a range of electrical power levels, including those higher than the capability of the spacecraft. Yet, our calculations hint at the possible effects

of design trade-offs on the impact speed. Third, our calculations allowed the launch angles to vary over a wide range and did not limit them to realistic limits. Due to these limitations, we do not make specific mission recommendations but only highlight some possibilities identified by the algorithm. With these caveats, we have demonstrated the utility of a simplified and parallelized genetic algorithm to evaluate the effect of on-board thrusters for impact missions.

Author Contributions: Conceptualization, K.S.; methodology, K.S. and S.A.G.; software, S.A.G., A.S.O., M.D.L. and N.C.T.; validation, K.S., S.A.G., N.C.T. and M.D.L.; formal analysis, K.S., S.A.G., N.C.T. and M.D.L.; investigation, N.C.T., M.D.L. and A.S.O.; resources, K.S. and S.A.G.; data curation, K.S., N.C.T. and M.D.L.; writing—original draft preparation, K.S.; writing—review and editing, K.S. and S.A.G.; visualization, K.S.; supervision, K.S. and S.A.G.; project administration, K.S. and S.A.G.; funding acquisition, K.S. and S.A.G. All authors have read and agreed to the published version of the manuscript.

Funding: NASA Washington Space Grant: NNX15AJ98H S000005.

Acknowledgments: Benjamin Michael, Mateo Reynoso Roman, and Lauren Taylor contributed to the early stages of this project. The authors thank Justin Atchinson for insights about the DART mission. This work was done with the support of the NASA Washington Space Grant Consortium and the NVIDIA Corporation's GPU hardware donation.

Conflicts of Interest: The authors declare no conflict of interest.

Nomenclature

The following abbreviations are used in this manuscript:

a_{th}	Acceleration of the spacecraft due to thrust (AU s^{-2})
f_{coast}	Function used to optimize coasting (#)
F_{th}	Thrust exerted on the spacecraft (kg AU s^{-2})
m_{sp}	Mass of the spacecraft (kg)
r, θ, z	Radial, angular, and off-plane position of the spacecraft (AU, rad, AU)
$\varkappa$	Magnitude of separation of the spacecraft from the Sun (AU)
ESOI	Earth's sphere of influence
T	Trip time from leaving ESOI to impact (s)
V_r, V_θ, V_z	Radial, tangential, and off-plane velocity of the spacecraft (AU/s)
α	Angular location in the ecliptic plane at ESOI (rad)
β, ζ	In-plane and off-plane angles of velocity at ESOI (rad)
γ, τ	In-plane and off-plane directions of thrust (rad)
η	Thrust efficiency (#)
Φ	Fraction of "parents" chosen based on proximity vs. impact speed (#)
ψ	Input function to f_{coast} (rad)

References

1. Stahl, B.; Braun, R. Low-Thrust Trajectory Optimization Tool to Assess Options for Near-Earth Asteroid Deflection. In Proceedings of the AIAA/AAS Astrodynamics Specialist Conference and Exhibit, Honolulu, HI, USA, 18–21 August 2008; AIAA: Honolulu, HI, USA, 2008; p. 6255. [CrossRef]
2. Sankaran, K.; French, A.; Gady, S.; Wisniewski, T.; Woodkey, M. Evaluation of Electric Propulsion Systems for Asteroid and Comet Sample-Return Missions. In Proceedings of the AIAA/ASME/SAE/ASEE Joint Propulsion Conference, Cleveland, OH, USA, 28–30 July 2014; AIAA: Cleveland, OH, USA, 2014; p. 3720. [CrossRef]
3. Englander, J.; Conway, B. An Automated Solution of the Low-Thrust Interplanetary Trajectory Problem. *J. Guid. Control Dyn.* **2016**, *40*, 15–27. [CrossRef] [PubMed]
4. Casalino, L.; Simeoni, F. Indirect optimization of asteroid deflection missions with electric propulsion. *J. Guid. Control Dyn.* **2012**, *35*, 423–433. [CrossRef]
5. Kantsiper, B. The Double Asteroid Redirection Test (DART) mission electric propulsion trade. In Proceedings of the 2017 IEEE Aerospace Conference, Big Sky, MT, USA, 4–11 March 2017; IEEE: Big Sky, MT, USA, 2017; pp. 1–7. [CrossRef]
6. Knittel, J.; Englander, J.; Ozimek, M.; Atchison, J.; Gould, J. Improved Propulsion Modeling for Low-Thrust Trajectory Optimization. In Proceedings of the AAS/AIAA Space Flight Mechanics Meeting, San Antonio, TX, USA, 5–9 February 2017; AAS: San Antonio, TX, USA, 2017; pp. 1–19.

7. Jean, I.; Misra, A.; Ng, A. Controlled Spacecraft Trajectories in the Context of a Mission to a Binary Asteroid System. *J. Astronaut. Sci.* **2021**, *68*, 38–70. [CrossRef]
8. Cheng, A.; Michel, P.; Reed, C.; Galvez, A.; Carnelli, I. DART: Double Asteroid Redirection Test. In Proceedings of the European Planetary Science Congress (EPSC), Madrid, Spain, 23–28 September 2012; Volume 7, p. 935.
9. Atchison, J.; Ozimek, M.; Kantsiper, B.; Cheng, A. Trajectory options for the DART mission. *Acta Astronaut.* **2016**, *123*, 330–339. [CrossRef]
10. Sarli, B.; Ozimek, M.; Atchison, J.; Englander, J.; Barbee, B. NASA Double Asteroid Redirection Test (DART) Trajectory Validation and Robustness. In Proceedings of the AAS/AIAA Space Flight Mechanics Meeting, San Antonio, TX, USA, 5–9 February 2017; AAS: San Antonio, TX, USA, 2017; pp. 1–17.
11. Ozimek, M.; Atchison, J. NASA Double Asteroid Redirection Test (DART) Low-Thrust Trajectory Concept. In Proceedings of the AAS/AIAA Space Flight Mechanics Meeting, San Antonio, TX, USA, 5–9 February 2017; AAS: San Antonio, TX, USA, 2017; pp. 1–20.
12. Sarli, B.; Atchison, J.; Ozimek, M.; Englander, J.; Barbee, B. Double Asteroid Redirection Test Mission: Heliocentric Phase Trajectory Analysis. *J. Spacecr. Rocket.* **2019**, *56*, 546–558. [CrossRef]
13. Patterson, M.; Foster, J.; Haag, T.; Rawlin, V.; Soulas, G.; Roman, R. NEXT: NASA's Evolutionary Xenon Thruster. In Proceedings of the AIAA/ASME/SAE/ASEE Joint Propulsion Conference, Indianapolis, IN, USA, 7–10 July 2002; AIAA: Indianapolis, IN, USA, 2002; p. 3832. [CrossRef]
14. Janin, G.; Gómez-Tierno, M. The Genetic Algorithms for Trajectory Optmization. In Proceedings of the 36th Congress of the International Astronautical Federation (IAF-85), Stockholm, Sweden, 7–12 October 1985; p. 244.
15. Hartmann, J.; Coverstone-Carroll, V.; Williams, S. Optimal Interplanetary Spacecraft Trajectories via a Pareto Genetic Algorithm. *J. Astronaut. Sci.* **1998**, *46*, 267–282. [CrossRef]
16. Vavrina, M.; Englander, J.; Philiips, S.; Hughes, K. Global, Multi-Objective Trajectory Optmization with Parametric Spreading. In Proceedings of the AAS/AIAA Space Flight Mechanics Meeting, San Antonio, TX, USA, 5–9 February 2017; AAS: San Antonio, TX, 2017; pp. 1–20.
17. Darani, S.; Abdelkhalik, O. Space Trajectory Optmization Using Hidden Genes Genetic Algorithms. *J. Spacecr. Rocket.* **2018**, *55*, 764–774. [CrossRef]
18. Van Noord, J. Lifetime Assessment of the NEXT Ion Thruster. In Proceedings of the AIAA/ASME/SAE/ASEE Joint Propulsion Conference, Cincinnati, OH, USA, 8–11 July 2007; AIAA: Cincinnati, OH, USA, 2007; p. 5274. [CrossRef]
19. Fisher, J.; Ferriauolo, B.; Hertel, T.; Monheiser, J.; Barlog, C.; Allen, M.; Myers, R.; Hoskins, A.; Bontempo, J.; Nazario, M.; et al. NEXT-C Flight Ion Propulsion System Development Status. In Proceedings of the International Electric Propulsion Conference (IEPC), Atlanta, GA, USA, 8–12 October 2017; ERPS: Atlanta, GA, USA, 2017; p. 218.
20. Abdelkhalik, O.; Taheri, E. Approximate On-Off Low-Thrust Space Trajectories Using Fourier Series. *J. Spacecr. Rocket.* **2012**, *49*, 962–965. [CrossRef]
21. Sankaran, K.; Hamming, B.; Grochowski, C.; Hoff, J.; Spaun, M.; Rollins, M. Evaluation of Existing Electric Propulsion Systems for the OSIRIS-REx Mission. *J. Spacecr. Rocket.* **2013**, *50*, 1292–1295. [CrossRef]
22. Stefano, I.; Cappuccio, P.; Iess, L. The BepiColombo solar conjunction experiments revisited. *Class. Quantum Gravity* **2020**, *38*, 055002. [CrossRef]
23. Dormand, J.R.; Prince, P.J. A family of embedded Runge-Kutta formulae. *J. Comput. Appl. Math.* **1980**, *6*, 19–26. [CrossRef]